The Cryosphere Discuss., doi:10.5194/tc-2016-99, 2016
Manuscript under review for journal The Cryosphere
Published: 23 May 2016

The Cryosphere Discussions
Open Access
EGU

Spatial variability in mass change of glaciers in the Everest region, central Himalaya, between 2000 and 2015

Owen King[1], Duncan J. Quincey[1], Jonathan L. Carrivick[1], Ann V. Rowan[2]

[1]School of Geography and water@leeds, University of Leeds, Leeds, LS2 9JT, UK.

[2]Department of Geography, University of Sheffield, Sheffield, S10 2TN, UK.

Correspondence to: gy08ok@leeds.ac.uk

Abstract. The mass balance of the majority of Himalayan glaciers is currently negative, and has been for several decades. Region wide averaging of mass change estimates has masked any catchment or glacier scale variability in glacier recession, thus the role of a number of glaciological processes in glacier wastage remains poorly understood. In this study, we quantify surface lowering and mass loss rates for the ablation areas of 32 glaciers in different catchments across the Everest region, and specifically examine the role of glacial lakes in glacier mass change. We then assess how future ice loss is likely to differ depending on glacier hypsometry. Spatially variable ice loss is observed within and between the Dudh Koshi and Tama Koshi catchments and glaciers that flow onto the Tibetan Plateau. Surface lowering rates on glaciers flowing onto the Tibetan Plateau are 54 % and 19 % greater than those flowing southward into the Dudh Koshi and Tama Koshi catchments, respectively. Surface lowering rates of up to –3.78 ± 0.26 m a^{-1} occurred on some lacustrine terminating glaciers, although glaciers with small lakes showed rates of lowering comparable with those that terminate on land. We suggest that such a range reflects glacial lakes at different stages of development, and that rates of mass loss are likely to increase as glacial lakes expand and deep water calving begins to occur. Hypsometric data reveal a coincidence of the altitude of maximum surface lowering and the main glacier hypsometry in the Dudh Koshi catchment, thus a large volume of ice is readily available for melt. Should predicted CMIP5 RCP 4.5 scenario warming (0.9-2.3 ºC by 2100) occur in the study area, 19-30, 17-50 and 14-37 % increases in the total glacierised area below the Equilibrium Line Altitude will occur in the Dudh Koshi and Tama Koshi catchments, and on the Tibetan Plateau. Comparison of our data with a conceptual model of Himalayan glacier shrinkage confirms the presence of three distinct process regimes, with all glaciers in our sample now in a state of accelerating mass loss and meltwater storage.

Keywords: Himalaya, glacier mass, debris-cover, Everest region, glacial lakes

The Cryosphere Discuss., doi:10.5194/tc-2016-99, 2016
Manuscript under review for journal The Cryosphere
Published: 23 May 2016

1. Introduction

The Himalaya holds the largest store of glacier ice outside of the polar ice sheets. Estimates of Himalayan ice volume range from 2,300 km^3 to 7,200 km^3 (Frey et al., 2014 and references within) distributed amongst more than 54,000 glaciers (Bajracharya et al., 2015). The current mass balance of Himalayan glaciers is predominantly negative, with accelerating mass loss having been observed over the past few decades (Bolch et al., 2012; Thakuri et al., 2014). This mass loss is occurring because of a combination of processes. Shrestha et al. (1999) show a rise in the mean annual air temperature of 0.057 °C/yr across the Himalaya between 1971 and 1994. Bollasina et al. (2011) show a reduction in total precipitation (–0.95 mm day^{-1}) amounting to 9 to 11% of total monsoon rainfall over a broad area of northern India between 1950 and 1999. Bhutiyana et al. (2010) show both decreasing total precipitation and a changing precipitation phase, with a lower proportion of precipitation falling as snow across the northwest Himalaya between 1996 and 2005. The snow cover season has been shortening as a result (Pepin et al., 2015). Under different climate scenarios, ice melt from the region may contribute 8.7–17.6 mm of sea level rise by 2100 (Huss and Hock, 2015).

Recent studies have identified spatial heterogeneity in mass loss across the Himalaya (Kääb et al., 2012; Gardelle et al., 2013). Glaciers in the Spiti Lahaul, in the western Himalaya, are losing mass most quickly (Kääb et al., 2012), whilst glaciers in the Eastern Himalaya (Bhutan, Hengduan Shan) and central Himalaya appear to be more stable (Gardelle et al., 2013). The anomalous balanced, or even slightly positive, glacier mass budget in the Karakoram is well documented (Kapnick et al., 2015). Prolonged mass loss from Himalayan glaciers may cause diminishing discharge of the largest river systems originating in the region (Immerzeel et al., 2010; Lutz et al., 2014), thereby impacting on Asian water resources in the long-term.

Few previous studies have assessed the variability of glacier mass loss within catchments (Pellicciotti et al., 2015). Nuimura et al. (2012) examined the altitudinal distribution of glacier surface elevation change in the Khumbu region, Nepal, and found similar surface lowering rates over debris-free and debris-covered glacier surfaces. Gardelle et al. (2013) detected enhanced thinning rates on lacustrine terminating glaciers in Bhutan, West Nepal, and the Everest region, but did not make an explicit comparison with land-terminating glacier recession rates. Benn et al. (2012) proposed a conceptual model of Himalayan glacier recession that included important thresholds between regimes of ice dynamics and mass loss at different stages of lake development. Benn et al. (2012) also suggested idealised mass balance curves and equilibrium line altitudes (ELAs) that

The Cryosphere Discuss., doi:10.5194/tc-2016-99, 2016
Manuscript under review for journal The Cryosphere
Published: 23 May 2016

represent each of these regimes and in turn indicate likely future ice loss given sustained climatic forcing. A direct comparison of mass loss data and the model of Benn et al. (2012) is yet to be made, however, and it thus remains untested.

In this work, we aim to quantify glacier surface lowering rates in three major catchments of the central Himalaya and assess the glacier-scale variability of ice loss within and between catchments. We specifically examine the rate of ablation area mass loss, hypsometry and total area change of each glacier and compare those terminating in a glacial lake with those terminating on land. We use these data together with climatic data from the region to define the major mechanisms driving ice mass loss, and to assess scenarios of likely future ice loss from our sample of glaciers.

2. Study area

We studied glaciers in three catchments of the Everest region (Figure 1), spanning both Nepal and Tibet (China). Two of the catchments, the Dudh Koshi and the Tama Koshi, are located in north-eastern Nepal and drain the southern flank of the Himalaya. The third catchment is located to the north of the divide, and the glaciers drain north into Tibet (China). Most glaciers in the studied catchments are characterised by long (10–15 km), low-slope angle, debris-covered tongues that are flanked by large (tens of metres high) moraine ridges (Hambrey et al., 2008). Some glaciers have accumulation areas several kilometres wide, accumulation zones that reach extreme altitudes (up to 8000 m in the case of the Khumbu), whereas others sit beneath mountain massifs (e.g. Lhotse and the Lhotse face), are fed almost exclusively by avalanches and are less than 1 km in width for their entire length.

Of the 278 glaciers in the Dudh Koshi catchment, the largest 40 are debris-covered and comprise 70 % of the total glacierised area (482 km^2- Bajracharya and Mool, 2009). Here, the total area of glacier surface covered by debris has increased since the 1960s (Thakuri et al., 2014) and several previous studies have published surface lowering data for the catchment indicating accelerating surface lowering rates over recent decades (e.g. Bolch et al., 2011). We select nine of the largest glaciers for analysis given that they provide the greatest volume of meltwater to downstream areas. There are a total of 80 glaciers in the Tama Koshi catchment covering a total area of 110 km^2 (Bajracharya et al., 2015). We again selected the largest nine glaciers for analysis based on relative contributions to river flow. This is a poorly studied catchment, perhaps best known for the existence of Tsho Rolpa glacial lake, which underwent partial remediation during the 1990s (Reynolds, 1999). The fourteen

The Cryosphere Discuss., doi:10.5194/tc-2016-99, 2016
Manuscript under review for journal The Cryosphere
Published: 23 May 2016

glaciers within our sample that flow onto the Tibetan Plateau all contribute meltwater to the Pumqu river catchment, which covers an area of 545 km^2 (Che et al., 2014). Debris cover is less prevalent on glaciers of the Pumqu catchment, and terminus recession has caused a 21 % of glacier area loss since 1970 (Jin et al., 2005; Che et al., 2014). There is relatively little information on glacier equilibrium line altitudes (ELAs) for any of the studied catchments; those in the Dudh Koshi were estimated to be at around 5600 m a.s.l. in the early 2000s (Asahi, 2001), and those in the Rongbuk catchment were estimated between 5800 and 6200 m a.s.l. for the period 1974–2006 (Ye et al., 2015).

Gardelle et al. (2011) identified 583 supraglacial ponds and lakes in the Everest region. Some of the largest glacial lakes in this region have been expanding in recent decades (Sakai et al., 2000; Che et al., 2014; Somos-Valenzuela et al., 2014). This increased meltwater ponding at glacier termini has potential to affect ice dynamics and down-valley meltwater and sediment fluxes (Carrivick and Tweed, 2013) as well as causing a hazard to populations living downstream. Several of the lakes have burst through their moraine dams in previous decades causing rapid and extensive flooding downstream; the best studied outburst floods are those from Nare glacier in 1977 (Buchroithner et al., 1982) and from Dig Tsho in 1985 (Vuichard and Zimmerman, 1987).

3. Data sources and methods

3.1 Data sources

3.1.1 Digital elevation models

Our reference elevation dataset across all three catchments is the Shuttle Radar Topographic Mission (hereafter SRTM) version 3.0, non-void filled, 1 arc second digital elevation model (hereafter DEM). This dataset was acquired in February 2000 and was released at 30 m resolution in late 2014 (USGS, 2016). SRTM employed two SAR systems, a 5.6 cm C-band and a 3.1 cm X-band system, with the main objective of obtaining single-pass interferometric SAR imagery to be used for DEM generation on a near global scale (56˚S to 60˚ N- 80% of the planet's surface) with targeted horizontal and vertical accuracies of 16 m and 20 m, respectively. Farr et al. (2007) report horizontal and vertical accuracies of better than 10 m for most regions globally.

Our 2014/2015 elevation dataset comprises a number of high resolution (8 m grid) DEMs generated Ohio State University and distributed online by the Polar Geospatial Centre at the University of Minnesota that provide coverage of an extended area around the Everest region (Table 2). These stereo-photogrammetric DEMs have

The Cryosphere Discuss., doi:10.5194/tc-2016-99, 2016
Manuscript under review for journal The Cryosphere
Published: 23 May 2016

been generated using a Surface Extraction with TIN-based Search-space Minimization (hereafter SETSM) algorithm from Worldview 1, 2 and 3 imagery (Noh and Howat, 2015). The SETSM algorithm is designed to automatically extract a stereo-photogrammetric DEM from image pairs using only the Rational Polynomial Coefficients (RPCs) as geometric constraints. The geolocation accuracy of RPCs without ground control for Worldview 1 and 2 data is 5 m (Noh and Howat, 2015) which may ultimately result in matching failure. The SETSM algorithm updates RPCs to mitigate this error and produces DEMs with an accuracy of ± 4 m in X, Y and Z directions (Noh and Howat, 2015). SETSM DEMs are gap-filled using a natural neighbour interpolation; we removed these pixels before DEM differencing and the calculation of mass loss rates across the ablation areas of individual glaciers.

Over two small areas of the Dudh Koshi (over the lower reaches of the Bhote Kosi and Melung glaciers) the SETSM DEMs contained data gaps. To complete coverage of DEMs over these glaciers we generated ASTER DEMs and used the surface to cover elevation bands across these glaciers where no data were available from the SETSM grids. We used ERDAS Imagine (2013) to generate ASTER DEMs with ground control points (GCPs) matched between features in the ASTER imagery and the high resolution imagery available in Google Earth. We used a large number of GCPs (45) and tie points (> 75) to minimise the root mean squared (RMS) error of GCP positions. All SETSM and ASTER DEMs were resampled to a 30 m resolution to match that of the SRTM data before any differencing was carried out.

3.1.2 Glacier outlines

Glacier outlines were downloaded from the Global Land Ice Measurement from Space (GLIMS) Randolph Glacier Inventory (RGI) Version 5.0 (Liu and Guo, 2014; Bajracharya et al., 2014; Racoviteanu and Bajracharya, 2008) and modified to account for changes in glacier extent between our datasets. Adjustments were made based on two Landsat scenes closely coinciding in acquisition with the DEM data. The 2000 Landsat scene was acquired by the ETM+ sensor and thus has a single 15 m resolution panchromatic band and six 30 m multispectral bands. The 2014 scene was acquired by the OLI sensor and also has a single 15 m panchromatic band as well as eight 30 m multispectral bands. Both scenes were pan-sharpened to match the resolution of the multispectral bands to that of the panchromatic band before glacier outlines were adjusted. Adjustments were limited to correcting changes in glacier frontal position and changes along the lateral margins because of surface lowering.

The Cryosphere Discuss., doi:10.5194/tc-2016-99, 2016
Manuscript under review for journal The Cryosphere
Published: 23 May 2016

3.2 Highlighted glaciers

The differencing of DEMs yielded data on glacier geometry change throughout the study area, and we highlight 32 of the largest glaciers (Figure 1) in this work. These glaciers vary in aspect and altitudinal range (Table 2). We include 5 debris-free glaciers from the Tibetan Plateau and 28 valley glaciers that are all at least partially covered by debris layers thought to be at least several decimetres thick (Rounce and McKinney, 2014; Rowan et al., 2015). We classify nine glaciers from the sample as lacustrine terminating, where the glacier termini and glacial lakes are actively linked. While both the Gyabrag and Rongbuk glaciers are associated with a proglacial lake we do not consider either as lacustrine terminating. In the case of the Gyabrag Glacier the ice is now separated from the lake by a large outwash plain. In the case of the Rongbuk Glacier, the lake is supraglacial and far up-glacier from its terminal region and thus does not currently influence the recession of the terminus of the glacier. The expanding Spillway Lake at the terminus of Ngozumpa Glacier (Thompson et al., 2012) is currently of limited depth, and is unlikely to affect glacier dynamics in its current state so we also exclude the Ngozumpa from the lacustrine terminating category.

3.3 DEM correction

3.3.1 Stereoscopic DEMs

We followed the three-step correction process of Nuth and Kääb (2011), through which biases inherent in stereoscopic DEMs can be corrected. We assessed and corrected where necessary for: (i) mismatch in the geo-location of the modern DEMs versus the reference SRTM dataset (in x, y, and z direction); (ii) the existence of an elevation dependant bias, and; (iii) biases related to the acquisition geometry of the data. Each step was taken individually, so that separate error terms could be understood, rather than bundling them together as multiple regression based adjustments as previous studies have done, such as Racoviteanu et al. (2008) and Peduzzi et al (2010), for example. Corrections applied to DEMs where any one of the three biases were present included shifting of DEM corner coordinates, simple vertical shifting through addition or subtraction, and the fitting of linear and polynomial trends depending on the spatial variability of elevation differences across DEMs and through their elevation ranges. The largest shifts (tens of metres) were required in the z-direction to account for height above ellipsoid versus height above geoid differences between ASTER and SETSM DEMs and the SRTM DEM. Acquisition geometry related biases were detected in two SETSM strips (Table 3) and both ASTER scenes and were corrected for using first order trends taken along or cross the satellite track.

The Cryosphere Discuss., doi:10.5194/tc-2016-99, 2016
Manuscript under review for journal The Cryosphere
Published: 23 May 2016

3.3.2 SRTM DEM correction

Some studies have suggested that the SRTM dataset may underestimate glacier surface elevations because of C-band radar wave penetration into snow and ice (Rignot et al., 2001). Gardelle et al. (2013) assessed the magnitude of C-band penetration over various test sites in the Himalaya, finding variable bias across different regions, from 3.4 m in the Karakoram, to 1.4 m in the Everest region. Due to the spatially variable snowpack conditions present across glaciers and glacier clusters at any point in time, and the paucity of data available on such conditions (Kääb et al., 2015), radar penetration corrections are rarely applied to interferometric DEMs (Nuth and Kääb, 2011). For these reasons we accounted for a potential 1.4 m bias in our SRTM data (after Gardelle et al., 2013) by adding 0.1 m a^{-1} to our estimates of uncertainty.

Berthier et al. (2006) suggested that the extreme topography present in mountain regions is poorly replicated in coarse-resolution DEMs such as the SRTM DEM. Different studies have applied positive or negative corrections to the SRTM DEM (Berthier et al., 2007; Larsen et al., 2007), depending on the severity of the terrain at their respective study sites. Inspection of DEM differences across the study site showed no clear relationship between elevation differences and altitude (see supplementary information), thus no elevation dependant correction was applied to the SRTM data.

3.4 DEM differencing uncertainty

The co-registered DEMs were differenced to yield surface elevation change and outlying values greater than ± 60 m were filtered from the resulting data.

To understand the uncertainty associated with surface elevation change, we calculated the standard error of the mean elevation change (Gardelle et al., 2013). Using the standard deviation of stable terrain differences alone as an estimate of uncertainty is insufficient because this value would contain both noise and real topographic change (Bolch et al., 2011; Gardelle et al., 2013), and is averaged over larger areas (Berthier et al., 2010). The approach of Bolch et al. (2011) was followed here. The standard error (SE) can be calculated through:

$$SE = \frac{StDev_{stable}}{\sqrt{n_{diff}}} \quad (1)$$

The Cryosphere Discuss., doi:10.5194/tc-2016-99, 2016
Manuscript under review for journal The Cryosphere
Published: 23 May 2016

Where *StDev stable* is the standard deviation of stable terrain differences and *n diff* is the number of pixels included in DEM differencing. *n diff* is less than the total number of pixels in the original DEMs, and must also consider pixel size and spatial autocorrelation. *n diff* was calculated following Gardelle et al. (2013) using:

$$n_{diff} = \frac{n_{tot} \cdot PS}{2d} \quad (2)$$

Where *ntot* is total pixel count of the original DEM, *PS* is pixel size (30 m) and *d* is the distance of spatial autocorrelation, a measure of how similar local objects are, for the SETSM and ASTER DEMs. 160m and 600 m, or 20 pixels, was used here as in Bolch et al. (2011). Elevation change uncertainty was then estimated using SE and the mean elevation differences (MED) over stable, non-glacier areas:

$$e = \sqrt{SE^2 + MED^2} \quad (3)$$

While we appreciate this approach does not provide an entirely independent estimate of uncertainty, and additionally combines both random and systematic errors, in the absence of ground control data we take it to be the best available measure. The resulting uncertainty estimates of surface elevation change for each DEM against the SRTM dataset over the study period are listed in Table 3. Values of standard deviation are in line with other studies (e.g. Berthier et al., 2006; Bolch et al., 2011) and are typical of DEM differencing studies over rough topography (Kääb, 2005). Our estimates of standard error are generally small, and all lower than the annual surface lowering rates over glacier surfaces (Table 3).

3.5 Hypsometric analysis

Glacier hypsometry, the distribution of glacier area over altitude, is governed by valley shape, relief and ice volume distribution (Jiskoot et al., 2009). It is important for long-term glacier response because it defines the distribution of mass with elevation and thus determines how the glacier responds to changes in elevation-dependent temperature (Furbish and Andrews, 1984). To assess glacier hypsometry, we used pan-sharpened Landsat ETM+ and Landsat OLI scenes from the same two time periods as the two DEM sets (Table 1) and, where necessary, modified the Randolph Glacier Inventory (RGI) to create glacier outlines from the different epochs. We split these glacier extents into segments covering 100 m elevation ranges, and calculated the area of each segment. To assess the overall area change of each glacier, we compared the undivided, total area of digitised glacier outlines from each epoch. We followed the approach of Jiskoot et al. (2009) to categorise each glacier or the population of glaciers in each catchment according to a hypsometric index (HI), where:

The Cryosphere Discuss., doi:10.5194/tc-2016-99, 2016
Manuscript under review for journal The Cryosphere
Published: 23 May 2016

$$HI = \frac{(H_{max} - H_{med})}{(H_{med} - H_{min})} \quad (4)$$

and H_{max} and H_{min} are the maximum and minimum elevations of the glacier, and H_{med} the elevation that divides the glacier area in half (Jiskoot et al., 2009). Glaciers were grouped into five HI categories: 1- HI < –1.5, very top heavy; 2- HI –1.2 to –1.5, top heavy; 3- HI –1.2 to 1.2, equidimensional; 4- HI 1.2 to 1.5, bottom heavy; and 5- HI > 1.5, very bottom heavy. Top heavy glaciers store more ice at higher elevation, for example in broad accumulation zones, whereas bottom heavy glaciers have small accumulation zones and long tongues.

3.6 Mass loss calculations

We did not generate mass balance estimates because of the incomplete coverage of DEMs over the high-elevation accumulation areas of a number of glaciers, mainly due to data voids in the SRTM DEM. Instead, we estimated mass loss from the ablation zones of the 32 glaciers to allow comparison between different catchments and between land- and lacustrine-terminating glaciers. As in previous mass loss studies in the Himalaya (Bolch et al., 2011; Gardelle et al., 2013) a conversion factor of 900 kg m^{-3} was used to account for the density of glacier ice for all glaciers in the sample. We assigned an additional 7 % to mass loss uncertainty estimates to account for error in the density conversion (Huss, 2013). The mass loss estimates generated for lacustrine terminating glaciers are slight underestimates because, with no information available on bed topography, we cannot account for ice that has been replaced by water during lake expansion. Surface lowering and mass loss rates for these glaciers have been measured from 2014/2015 calving fronts as a result.

4. Results

4.1 Surface lowering

There is considerable variability in the mean surface lowering rates across each catchment, in the surface lowering rates of adjacent glaciers within catchments (Figures 3 and 4), and through the altitudinal range of highlighted glaciers (Figures 5 and 6). Catchment-wide surface lowering rates are contrasting on the northern and southern flank of the Himalaya. Mean glacier surface lowering rates in the Tama Koshi and Dudh Koshi catchments were 0.80 ± 0.35 m a^{-1} and 0.62 ± 0.37 m a^{-1} over their ablation zones. The ablation zones of glaciers flowing onto the Tibetan Plateau lowered by 0.95 ± 0.30 m a^{-1} on average (Table 4).

The Cryosphere Discuss., doi:10.5194/tc-2016-99, 2016
Manuscript under review for journal The Cryosphere
Published: 23 May 2016

The presence of a glacial lake altered the gradient of surface lowering over glacier surfaces. Mass loss rates increased down glacier on highlighted lacustrine terminating glaciers, whereas surface lowering was negligible around the terminus of most land terminating glaciers. Only in the Tama Koshi catchment, where glacial lakes are largest, is there a clear contrast in the surface lowering rates seen on lacustrine terminating versus land terminating glaciers (Table 4). The ablation zones of land terminating glaciers in the Tama Koshi lowered by 0.47 ± 0.18 to 0.72 ± 0.54 m a^{-1}; the mean surface lowering rate was 0.56 ± 0.29 m a^{-1}. Surface lowering rates ranged between 0.78 ± 0.66 and 1.55 ± 0.26 m a^{-1} on lacustrine terminating glaciers in the Tama Koshi catchment; the mean surface lowering rate was 1.10 ± 0.43 m a^{-1}. The surface lowering rates of lacustrine terminating and land terminating glaciers are broadly similar in the Dudh Koshi catchment and on the Tibetan Plateau (Table 4). Surface lowering rates ranged between 0.31 ± 0.26 and 0.84 ± 0.16 m a^{-1} on land terminating glaciers in the Dudh Koshi catchment; the mean surface lowering rate was 0.60 ± 0.27 m a^{-1} (Table 4). The mean surface lowering rate of lacustrine terminating glaciers in the Dudh Koshi catchment was 0.66 ± 0.27 m a^{-1}. The surfaces of land terminating, debris-covered glaciers flowing onto the Tibetan Plateau lowered by 0.64 ± 0.16 to 1.31 ± 0.18 m a^{-1}; the mean was 0.96 ± 0.32 m a^{-1}. This lowering rate is 60 % and 71 % greater than the mean lowering rate of land-terminating glaciers in the Dudh Koshi and Tama Koshi catchments.

The altitude at which maximum surface lowering rates occurred again seems to depend on glacier terminus type (Figures 5 and 6). Across all three catchments, substantial mass loss was pervasive over the middle portions of larger, land terminating glaciers (Figure 2). In the Dudh Koshi, surface lowering rates are at their highest (1.01 ± 0.27 m a^{-1}) around 5300 m a.s.l., although similar surface lowering rates occurred between 5100 and 5300 m a.s.l (Figure 5). In the Tama Koshi the highest rates of surface lowering (0.85 ± 0.35 m a^{-1}) occurred at around 5300 m a.s.l, with similar surface lowering rates occurring between 5000 and 5300 m a.s.l (Figure 5). On the Tibetan Plateau, the highest surface lowering rates were almost double those of the Tama Koshi or Dudh Koshi catchments. These rates occurred at ~ 5300 m a.s.l.; the mean glacier surface lowering rate was 1.68 ± 0.30 m a^{-1}. Surface lowering rates over glaciers on the Tibetan Plateau were higher than those in the Tama and Dudh Koshi catchments up to 5800 m a.s.l. (1.03 ± 0.30 m a^{-1}). Of note is the high surface lowering rates over clean ice areas high up on glaciers such as the Ngozumpa, Rongbuk, Gyabrag and Bhote Kosi (Figure 2). Surface lowering extended into tributary branches and the cirques of these largest glaciers. Individual glaciers showed much greater surface lowering rates, particularly on the Tibetan Plateau. The surface of the Gyabrag glacier

The Cryosphere Discuss., doi:10.5194/tc-2016-99, 2016
Manuscript under review for journal The Cryosphere
Published: 23 May 2016

lowered by an exceptional 3.40 ± 0.26 m a^{-1} between 5300 and 5400 m a.s.l (Figure 5) with a mean rate of 1.22 ± 0.26 m a^{-1} over the entire ablation area.

The terminus areas of lacustrine terminating glaciers lowered at a higher rate than all other glaciers across the Tama Koshi or Dudh Koshi catchments. The Yanong glacier in the Tama Koshi catchment shows the highest surface lowering rate (3.78 ± 0.26 m a^{-1}) near its terminus over the study period. Between 4600 m and 5000 m a.s.l., mean surface lowering rates of between 2.04 ± 0.34 m a^{-1} occurred on lacustrine terminating glaciers (Figure 6) compared to an average of 0.48 ± 0.29 m a^{-1} for land terminating glaciers over the same altitudinal range from the same catchments.

The lowest surface lowering rates have occurred over debris-free glaciers at high altitude (5600 – 6200 m a.s.l) on the Tibetan plateau. The mean surface lowering rate over these glaciers was 0.49 ± 0.42 m a^{-1} (Table 4).

4.2 Glacier area changes and hypsometry

4.2.1 Total area changes

Two different scenarios of ice area loss occurred over the study area during the last 15 years. Lacustrine terminating glaciers and clean ice glaciers all lost ice around their termini/ calving fronts (Figures 3 and 4) as glacial lakes expanded and termini retreated. On average, lacustrine terminating glaciers each lost 0.54 km^2 of ice over the 15 year study period. Drogpa Nagtsang reduced in size by 2.37 km^2 (9.12 % of its total area: Table 5) as the associated rapidly-forming lake expanded. 'Clean ice' glaciers lost 0.09 km^2 of ice (1.31 %) on average.

Land terminating glaciers in the Tama Koshi and Dudh Koshi catchments lost little area (0.14 km^2 and 0.09 km^2 on average, respectively) as their surfaces lowered rather than their termini retreating. Over these glaciers, any ice area loss was concentrated up-glacier, where their lateral margins dropped down inner moraine slopes and glacier tongues narrowed slightly. Glaciers flowing onto the Tibetan Plateau, whose surfaces lowered at the fastest rate over the study period, showed greater area loss, again mainly at their lateral margins. The total area of the Gyabrag glacier (Figure 3) reduced by 1.17 km^2 (3.32 %) over the study period.

4.2.2 Glacier hypsometry

The Cryosphere Discuss., doi:10.5194/tc-2016-99, 2016
Manuscript under review for journal The Cryosphere
Published: 23 May 2016

The distribution of ice with elevation varies widely among the three studied catchments. Glaciers of the Dudh Koshi catchment and on the Tibetan Plateau are typically very bottom heavy, with average HI scores of 2.63 and 2.34, respectively (Table 5). Glacier hypsometry is concentrated between 4800 and 5500 m (Figure 5) for the Dudh Koshi catchment, and between 5600 and 6500 m on the Tibetan Plateau. Notable exceptions are the Khumbu and Ngozumpa Glaciers which store ice in broad accumulations zones above 7000 m (Tables 2 and 4). The majority of glaciers in the Tama Koshi have an equi-dimensional hypsometry (mean HI of 1.14), with most ice stored between 5300 and 5800 m. Glaciers in the Tama Koshi have broader accumulation basins than in the Dudh Koshi catchment, and main glacier tongues are formed of multiple, smaller tributaries flowing from higher altitude in a number of cases (Figure 1). The mean hypsometry (Figure 6) of lacustrine terminating glaciers shows no distinctive morphology as the sample is composed of glaciers from all three catchments in the study area.

4.2.3 Approximate equilibrium line altitudes

The altitude at which surface lowering curves approach zero is a good indicator of the ELA of glaciers over a given study period (Nuth et al., 2007). Table 5 shows approximate ELAs for the glaciers in our sample. Using those ELAs the accumulation area ratio (AAR) (Dyurgerov et al., 2009) can be estimated for each glacier and this is a parameter strongly related to long-term mass balance (König et al., 2014). The ELAs of the glaciers we have surveyed in the Dudh Koshi catchment are above the altitudinal range within which 63 % of ice is stored in the catchment. In the Tama Koshi catchment, ELAs are higher than 64 % of glacierised area. Across the sample of Tibetan plateau glaciers, the highly variable ELAs are higher than 60 % of the glacierised area, excluding those we categorised as ‘clean ice’ glaciers.

5. Discussion

5.1 Variability in rates of ice loss across the orographic divide

The mean surface lowering rates measured over the ablation area of glaciers flowing northward onto the Tibetan Plateau, excluding those we classify as clean ice, are 54 % and 19 % greater than those for glaciers flowing southward into the Dudh Koshi and Tama Koshi catchments (Table 4), suggesting an additional or amplified process driving glacier change on the northern flank of the Himalaya. Maximum surface lowering rates (Figure 5) show an even greater divergence between these northward and southward-flowing glaciers. In this section we

The Cryosphere Discuss., doi:10.5194/tc-2016-99, 2016
Manuscript under review for journal The Cryosphere
Published: 23 May 2016

discuss possible topographic and climatic drivers of the difference in the rates of mass loss across the range divide.

The Indian summer monsoon delivers extremely large amounts of precipitation to the Everest region of Nepal, resulting in high glacier sensitivity to temperature (Rupper et al., 2012). The extreme topography in this region and the location of the orographic divide perpendicular to the prevailing monsoon result in rainfall peaks that are offset from the maximum elevations, with greatest rainfall occurring to the south of the divide and decreasing to the north across the Everest region (Bookhagen and Burbank, 2010). Around 449 mm a^{-1} of rainfall falls at the Pyramid research station (5000 m a.s.l.) at Khumbu Glacier (Salerno et al., 2015), whereas to the north at Dingri on the Tibetan Plateau (4300 m a.s.l.), 263 ± 84.3 mm a^{-1} of rainfall occurs annually (Yang et al., 2011). Snowfall may follow a similar across-range gradient to rainfall, although falling snow may be carried further into the range by prevailing winds from the south. However, no reliable measurements of snowfall exist in this region with which to compare these trends. The north-south precipitation gradient across the orographic divide promotes differences in the response of these glaciers to climate change, such that those to the north are relatively starved of snow accumulation (Owen et al., 2009) and exposed to greater incoming radiative fluxes under generally clearer skies. Therefore, as a result of the orographic precipitation gradient, those glaciers on the Tibetan Plateau are likely to have experienced sustained mass loss at greater rates than those glaciers to the south as temperatures have increased during the last century.

During the period of this study (2000–2015), mean annual air temperatures have increased and rainfall amounts appear to have decreased in the Everest region (Salerno et al., 2015). At the Pyramid Observatory at Khumbu Glacier in the Dudh Koshi catchment, increases in minimum (+0.07 °C/a), maximum (+0.009 °C/a) and mean (+0.044 °C/a) annual air temperatures above 5000 m a.s.l. were observed between 1994 and 2013 (Salerno et al., 2015). At Dingri on the Tibetan Plateau 60 km northeast of Mt. Everest, increases in minimum (+0.037 °C/a), maximum (+0.041 °C/a) and mean (+0.037 °C/a) annual air temperatures occurred over the same period (Salerno et al., 2015). Yang et al. (2011) found a clear relationship between increasing temperatures over time at Tingri and at temporary (operational between May 2007 and August 2008) weather stations on the Rongbuk and East Rongbuk glaciers, and suggest that the increases in temperature at Tingri have been replicated at glacierised altitudes. Snow accumulation appears to have recently decreased across the Everest region; Thakuri et al. (2014) showed a rapid ascent of the snow-line altitude in the Dudh Koshi between 1962 and 2011, and Kaspari et al. (2008) showed decreasing accumulation in the East Rongbuk Glacier Col (6518 m a.s.l.) since the 1970s.

The Cryosphere Discuss., doi:10.5194/tc-2016-99, 2016
Manuscript under review for journal The Cryosphere
Published: 23 May 2016

Khadka et al. (2014) suggest declining snow cover over the winter and spring months in the glacierised altitudinal ranges of the Tama Koshi catchment, between 2000 and 2009; a factor that may influence accumulation rates. These changes in air temperature and snowfall amount are likely to enhance glacier mass loss across the range in future.

5.2 The influence of glacial lakes on mass loss

The surface lowering rates we derive (Table 4) are comparable with those of other studies that have undertaken DEM differencing in different parts of our study area (Bolch et al., 2011; Nuimura et al., 2012; Gardelle et al., 2013). Nuimura et al. (2012) measured surface lowering rates of 0.87 m a^{-1} over glacier surfaces of low slope (<5 degrees) in part of the Dudh Koshi catchment, between 1992 and 2008. Bolch et al. (2011) generated a lengthy time series of DEMs covering Khumbu Glacier, and estimated a surface lowering rate of 0.79 m a^{-1} over the ablation area between 2002 and 2007. Over the same area and over an extended time period, we measured lowering rates of 0.84 m a^{-1}, suggesting an increase in the rate of ice loss. Gardelle et al. (2013) estimated surface lowering rates over debris-covered areas of 0.97 m a^{-1} and over 'clean ice' areas of 0.57 m a^{-1} for the period 1999 to 2011 across the Dudh Koshi catchment.

Only Nuimura et al. (2012) have directly compared surface lowering rates of lacustrine and land terminating glaciers in the study area, showing faster surface lowering rates over Imja and Lumding glaciers in the Dudh Koshi catchment. Our data confirm that lacustrine terminating glaciers can indeed thin at a much faster rate than land terminating glaciers, but the variability in the surface lowering rates over the 9 glaciers (Figure 6) we highlight suggests the fastest thinning rates occur in the later stages of lake development. Glaciers such as the Yanong and Yanong North, in the Tama Koshi catchment, sit behind large proglacial lakes and have shown extremely high surface lowering rates (3 m a^{-1} or more over their lower reaches). These glaciers are now relatively small and steep and no longer possess a debris-covered tongue, and so may represent the end-product of debris-covered glacier wastage described by Benn et al. (2012). In contrast, glaciers such as Duiya or Longmojian, on the Tibetan Plateau, currently have only small lakes at their termini, showed moderate area losses (0.44 and 0.5 km^2, or 4.28 and 2.07 % of total area, respectively) and surface lowering rates (1 to 2 m a^{-1}). Continued thinning of the terminal regions of these glaciers would lead to a reduction in effective pressure, an increase in longitudinal strain and therefore flow acceleration (Benn et al., 2007). The retreat of the calving front up-valley into deeper bed topography may also increase calving rates (Benn et al., 2007), and a combination of

The Cryosphere Discuss., doi:10.5194/tc-2016-99, 2016
Manuscript under review for journal The Cryosphere
Published: 23 May 2016

both of these processes would lead to enhanced ice loss. Very little surface velocity data exist for lacustrine terminating debris-covered glaciers. Only Quincey et al. (2009) measured high surface velocities (25 m/a^{-1} or more) over the Yanong glacier (their Figure 4, panel D), suggesting it is possible for lacustrine terminating glaciers to become more dynamic in the later stages of lake development in the Himalaya.

In exception, the surface lowering rates seen over Imja glacier (0.84 ± 0.51 m a^{-1} over the ablation area) are comparable with land-terminating glaciers close by (e.g. Lhotse 0.66 ± 0.51 m a^{-1}, Khumbu 0.84 ± 0.16 m a^{-1}), despite the presence of Imja Tsho at its terminus (Fujita et al., 2009). Somon-Valenzuala et al. (2014) show the presence of an ice foot below the calving front of Imja Tsho that may act to stabilise the calving front and limit ice loss. Somon-Valenzuala et al. (2014) also show an increase in the rate of lake expansion between 1992 and 2012, and an increase in the rate of surface lowering of glaciers in the region has previously been suggested (Bolch et al., 2011; Nuimura et al., 2012), thus Imja Tsho may be primed for further expansion.

5.3 Glacier stagnation

The pervasive nature of the heterogeneous pattern of surface lowering associated with ice cliff and melt pond development (Pellicciotti et al., 2015) over the lower reaches of a number of the larger glaciers we highlight (Figure 2) would suggest widespread stagnation of glacier tongues in our study area. Watson et al. (2016) have documented an increasing number and total area of supraglacial melt ponds over a number of glaciers in the Dudh Koshi catchment (Khumbu, Ngozumpa, Lhotse, Imja and Ama Dablam), since the early 2000's. We note a similar surface lowering pattern to that shown by Pellicciotti et al. (2015) on glaciers in the Langtang region over glaciers assessed by Watson et al. (2016), as well as over the Erbu, Gyachung, Jiuda, Shalong, and G1 glaciers (Figure 2). Similarly, Quincey et al. (2009) identified a number of glaciers with stagnant tongues in the Dudh Koshi catchment, and we would suggest a similar scenario for the glaciers listed above in the Tama Koshi catchment and on the Tibetan Plateau.

5.4 Susceptibility of glaciers to future mass loss

5.4.1 ELA ascent in response to warming

The coincidence of maximum surface lowering rates with the altitude of maximum hypsometry in the Dudh Koshi catchment (Figure 5) means a large amount of ice is readily available to sustain mass loss rates here. Surface lowering maxima in the Tama Koshi catchment presently occur at a slightly lower elevation range than

The Cryosphere Discuss., doi:10.5194/tc-2016-99, 2016
Manuscript under review for journal The Cryosphere
Published: 23 May 2016

the main hypsometric concentration, and across lower reaches of glacier tongues on the Tibetan Plateau, so glaciers in these catchments would be highly susceptible to accelerated ice loss should ELAs rise, albeit by varying amounts given the different altitudinal ranges of glaciers across the Himalayan range.

Our ELAs are above those estimated by Asahi (2001) and Kääb et al. (2012) for earlier epochs and similar to those estimated by Gardelle et al. (2013) over a similar study period to ours, suggesting that ELAs have indeed risen over recent decades. Considering lapse rates of 8.5 °C/km (Kattel et al., 2015) and 5.4 °C/km (Immerzeel et al., 2014) for catchments on the Northern and Southern slopes of the range, respectively, it is possible to estimate the elevation of ELAs given certain magnitudes of future warming. The Himalaya is expected to see 0.9 to 2.3 °C of warming up to the year 2100 (Collins et al., 2013), and we recalculate our ELAs for these upper and lower estimates.

Such temperature increases would cause a rise in ELA of between 165 and 425 m in the Dudh and Tama Koshi catchments, and between 107 and 270 m of ELA ascent over glaciers on the Tibetan Plateau. Catchment-averaged ELAs given 0.9 °C or 2.3 °C of warming are marked on Figure 4. A rise in ELAs would most significantly affect the Tama Koshi catchment glaciers, with 75 % and 95 % of glacier area being situated below the ELA given 0.9 °C and 2.3 °C of warming, respectively. This change in glacier area below the ELA is a 17 % or a 50 % increase compared with the current AAR. The more equidimensional hypsometry of Tama Koshi glaciers would mean exposure of greater glacier areas to ablation as ELAs rise through the large accumulation areas. The greater altitudinal range and smaller, avalanche fed accumulation zones of glaciers in the Dudh Koshi catchment and on the Tibetan Plateau would dampen the effects of a rise in ELA on glacier mass balance. Between 74 % and 81 % (a 19 % or 30 % increase, respectively) of glacier area would be below ELA in the Dudh Koshi, and between 68 % and 82 % on the Tibetan Plateau (14 % to 37 % increase) if the study area experienced such temperature increases, and thus we would expect particularly accelerated mass loss from glaciers in the Tama Koshi catchment.

5.4.2 Comparison with a conceptual model of glacier wastage

Benn et al. (2012) presented a conceptual model of Himalayan glacier wastage composed of three distinct process regimes each operating given certain climatic states. They suggested that transitions between these three process regimes marked major thresholds in glacier response to climatic forcing. By comparing the results from

The Cryosphere Discuss., doi:10.5194/tc-2016-99, 2016
Manuscript under review for journal The Cryosphere
Published: 23 May 2016

this study with the conceptual model of Benn et al. (2012), it is possible to identify at which stage of recession our highlighted glaciers, and which processes will drive glacier melt in the near future.

Figure 7 shows a comparison of the surface lowering curves we derive for the three major catchments in the study area, along with the 9 lacustrine terminating glaciers, and the conceptual mass balance curves proposed by Benn et al. (2012). There is a clear resemblance of the mean surface lowering curves generated for land-terminating glaciers in the three catchments of our study area and the mass balance curve of regime 2 outlined by Benn et al. (2012). The ablation gradients shown by lacustrine terminating glaciers are also very similar to regime 3 of Benn et al. (2012). Regime 2 is typified by accelerating ice loss and distributed water storage, and regime 3 is dominated by calving retreat and high amounts of water storage, according to Benn et al. (2012).

The transition of glaciers from regime 2 to regime 3 depends on the margins of a glacier being 'decoupled', specifically when the supply of supraglacial or englacial sediment at a glaciers margin is greater than the sediment transport capacity of meltstreams (Benn et al., 2003), and a large moraine dam is free to develop. The presence of such a moraine dam allows the formation of base level lakes and large scale calving events to occur, which is the main mechanism of ice loss in regime 3 of the Benn et al. (2012) model. Many of the glaciers we highlight possess a large terminal moraine and long, low surface gradient tongues, and thus seem primed for the transition from regime 2 to regime 3. We would expect an increase in mass loss rates of the lacustrine terminating glaciers that we highlight following the transition of glaciers from regime 2 to regime 3.

6 Conclusions

DEM differencing has revealed substantial mass loss from the ablation zones of many large, debris-covered glaciers in the central Himalaya over the last 15 years. Surface lowering in debris free areas of glacier tongues and over areas where ice cliffs are abundant has indicated decreased ice influx from accumulation zones and stagnation of the lower reaches of many large glaciers. Contrasting rates of surface lowering were observed in three different catchments around the Everest region. On the southern flank of the Himalaya, in the Tama Koshi and Dudh Koshi catchments, glacier surfaces lowered by 0.80 ± 0.35 m a^{-1} and 0.62 ± 0.37 m a^{-1} on average over their ablation zones. The ablation zones of glaciers flowing onto the Tibetan Plateau lowered by a mean of 0.95 ± 0.30 m a^{-1}. We suggest that the across-range contrast in annual precipitation total may have caused greater ice loss on the north flowing glaciers. The highest surface lowering rates we recorded were over the lower reaches of lacustrine terminating glaciers, reaching ~3.78 m a^{-1} on the Yanong North glacier. Mean

surface lowering rates of all lacustrine terminating glaciers in our sample were 0.91 ± 0.33 m a^{-1}, ranging from 0.54 ± 0.31 to 1.55 ± 0.26 m a^{-1}. The variability in the rates of mass loss from lacustrine terminating glaciers suggests that glacial lakes in the region are at different stages of expansion, and that accelerating mass loss is likely from several of these glaciers.

Glaciers of the Tama Koshi catchment have an equidimensional hypsometry and presently store large amounts of ice in broad accumulation zones. In contrast, glaciers in the Dudh Koshi and on the Tibetan Plateau are hypsometrically very bottom-heavy. They also have a greater altitudinal range than glaciers in the Tama Koshi catchment and thus have most ice stored in long, debris-covered tongues. In the Dudh Koshi catchment, the altitude of surface lowering maxima over the last 15 years is coincident with the altitude of maximum hypsometry. Thus a large area of ice is readily available for near-future ablation. A rise in ELA in response to predicted air temperature warming may cause a similar, though slightly less pronounced, scenario in the Tama Koshi catchment and on the Tibetan Plateau.

The ablation patterns and gradients found in this study support a model of three distinct process regimes proposed by Benn et al. (2012). All of the debris-covered glaciers that we have highlighted show evidence of the ablation processes in regimes 2 and 3 of the conceptual model of Benn et al. (2012). Mass loss rates will accelerate in the near future on glaciers that are presently with supraglacial lakes or small proglacial lakes, such as Drogpa Nagtsang, Duiya or Longmojian. Lake expansion over deeper bed topography will promote full depth calving and enhance ice loss on these glaciers. Glaciers showing signs of lake development, such as Ngozumpa, will lose more mass once their surfaces lower to the level of the base of their damming moraine, the drainage of ponded water is inhibited, and calving rates increase. Catchment wide ice mass loss rates will increase particularly rapidly when any rise in ELA coincides with the altitude of maximum surface lowering and the peak glacier hypsometry.

Author contribution

OK, DQ and JC designed the study. OK carried out all data processing and analysis. OK, DQ, JC and AR wrote the paper.

Acknowledgements

SETSM DEMs are available for download from http://www.pgc.umn.edu/elevation. The SRTM dataset is available from https://lta.cr.usgs.gov/SRTM1Arc. OK is a recipient of a NERC DTP PhD studentship. We are grateful for the comments of Benjamin Robson for his comments on an early version of the paper

References

Arendt, A., Bliss, A., Bolch, T., Cogley, J. G., Gardner, A. S., Hagen, J.-O., Hock, R., Huss, M., Kaser, G., Kienholz, C., Pfeffer, W. T., Moholdt, G., Paul, F., Radić, V., Andreassen, L., Bajracharya, S., Barrand, N.E., Beedle, M., Berthier, E., Bhambri, R., Brown, I., Burgess, E., Burgess, D., Cawkwell, F., Chinn, T., Copland, L., Davies, B., De Angelis, H., Dolgova, E., Earl, L., Filbert, K., Forester, R., Fountain, A. G., Frey, H., Giffen, B., Glasser, N. F., Guo, W. Q., Gurney, S., Hagg, W., Hall, D., Haritashya, U. K., Hartmann, G., Helm, C., Herreid, S., Howat, I., Kapustin, G., Khromova, T., König, M., Kohler, J., Kriegel, D., Kutuzov, S., Lavrentiev, I., LeBris, R., Liu, S. Y., Lund, J., Manley, W., Marti, R., Mayer, C., Miles, E. S., Li, X., Menounos, B., Mercer, A., Mölg, N., Mool, P., Nosenko, G., Negrete, A., Nuimura, T., Nuth, C., Pettersson, R., Racoviteanu, A., Ranzi, R., Rastner, P., Rau, F., Raup, B., Rich, J., Rott, H., Sakai, A., Schneider, C., Seliverstov, Y., Sharp, M., Sigurðsson, O., Stokes, C., Way, R. G., Wheate, R., Winsvold, S., Wolken, G., Wyatt, F., Zheltyhina, N. Randolph Glacier Inventory – A Dataset of Global Glacier Outlines: Version 5.0. Global Land Ice Measurements from Space, Boulder Colorado, USA. Digital Media. 2015.

Asahi, K. Inventory and recent variations of glaciers in the eastern Nepal Himalayas. Journal of the Japanese Society of Snow and Ice, 63, 159-169. 2001.

Bajracharya, S. R., Maharjan, S. B., Shrestha, F., Guo, W., Liu, S., Immerzeel, W. & Shrestha, B. The glaciers of the Hindu Kush Himalayas: current status and observed changes from the 1980s to 2010. International Journal of Water Resources Development, 31, 161-173. 2015.

Bajracharya, Samjwal (submitter); Shrestha, Finu; Bajracharya, Samjwal; Maharjan, SB; Guo, Wanqin (analyst(s)). GLIMS Glacier Database. Boulder, CO. National Snow and Ice Data Center. 2014.

Bajracharya, S. R. & Mool, P. Glaciers, glacial lakes and glacial lake outburst floods in the Mount Everest region, Nepal. Annals of Glaciology, 50, 81-86. 2009.

Benn, D. I., Kirkbride, M.P., Owen, L.A. & Brazier, V. 2003. Glaciated valley landsystems. In: Evans, D.J.A. (Ed.), Glacial Landsystems. Arnold, pp. 372–406.

Benn, D. I., Warren, C. R. & Mottram, R. H. Calving processes and the dynamics of calving glaciers. Earth-Science Reviews, 82, 143-179. 2007.

Benn, D. I., Bolch, T., Hands, K., Gulley, J., Luckman, A., Nicholson, L. I., Quincey, D., Thompson, S., Toumi, R. & Wiseman, S. Response of debris-covered glaciers in the Mount Everest region to recent warming, and implications for outburst flood hazards. Earth-Science Reviews, 114, 156-174. 2012.

Berthier, E., Arnaud, Y., Kumar, R., Ahmad, S., Wagnon, P. & Chevallier, P. Remote sensing estimates of glacier mass balances in the Himachal Pradesh (Western Himalaya, India). Remote Sensing of Environment, 108, 327-338. 2007.

Berthier, E., Arnaud, Y., Vincent, C. & Remy, F. Biases of SRTM in high-mountain areas: Implications for the monitoring of glacier volume changes. Geophysical Research Letters, 33. 2006.

Berthier, E., Scheifer, E., Clarke, G. K. C., Menounos, B. & Remy, F. Contribution of Alaskan glaciers to sea-level rise derived from satellite imagery. Nature Geoscience, 3, 92-95. 2010.

Bhutiyana, M.R. Kale, V.S. & Pawar, N.J. Climate change and the precipitation variations in the northwestern Himalaya: 1866-2006. International Journal of Climatology, 30, 535-548. 2010.

Bolch, T., Kulkarni, A., Kääb, A., Huggel, C., Paul, F., Cogley, J. G., Frey, H., Kargel, J. S., Fujita, K., Scheel, M., Bajracharya, S. & Stoffel, M. The State and Fate of Himalayan Glaciers. Science, 336, 310-314. 2012.

Bolch, T., Pieczonka, T. & Benn, D. I. Multi-decadal mass loss of glaciers in the Everest area (Nepal Himalaya) derived from stereo imagery. Cryosphere, 5, 349-358. 2011.

Bollasina, M. A., Ming, Y. & Ramaswamy, V. Anthropogenic Aerosols and the Weakening of the South Asian Summer Monsoon. Science, 334, 502-505. 2011.

Bookhagen, B. & Burbank, D. Towards a complete Himalayan hydrologic budget: The spatiotemporal distribution of snow melt and rainfall and their impact on river discharge. Journal of Geophysical Research, 115, p.F03019.

Buchroithner, M. F., Jentsch, G. & Wanivenhaus, B. Monitoring of recent geological events in the Khumbu area (Himalaya, Nepal) by digital processing of landsat MSS data. Rock mechanics, 15, 181-197. 1982.

Carrivick, J. L., & Tweed, F. S. Proglacial lakes: character, behaviour and geological importance. Quaternary Science Reviews, 78, 34-52. 2013.

Che, T., Xaio, L. & Liou, Y.-A. Changes in Glaciers and Glacial Lakes and the Identification of Dangerous Glacial Lakes in the Pumqu River Basin, Xizang (Tibet). Advances in Meteorology, 2014, 8. 2014.

Collins, M., R. Knutti, J. Arblaster, J.-L. Dufresne, T. Fichefet, P. Friedlingstein, X. Gao, W.J. Gutowski, T. Johns, G. Krinner, M. Shongwe, C. Tebaldi, A.J. Weaver and M. Wehner, 2013: Long-term Climate Change: Projections, Commitments and Irreversibility. In: Climate Change 2013: The Physical Science Basis. Contribution of Working Group I to the Fifth Assessment Report of the Intergovernmental Panel on Climate Change [Stocker, T.F., D. Qin, G.-K. Plattner, M. Tignor, S.K. Allen, J. Boschung, A. Nauels, Y. Xia, V. Bex and P.M. Midgley (eds.)]. Cambridge University Press, Cambridge, United Kingdom and New York, NY, USA

Dyurgerov, M., Meier, M. F. & Bahr, D. B. A new index of glacier area change: a tool for glacier monitoring. Journal of Glaciology, 55, 710-716. 2009.

Farr, T.G., Rosen, P.A., Carop, E., Crippen, R., Duren, R., Hensley, S., Korbick, M., Paller, M., Rodriguez, E., Roth, L., Seal, D., Shaffer, S., Shimada, J., Umland, J., Werner, M., Oskin, M., Burbank, D. & Alsdorf, D. The Shuttle Radar Topography Mission. Reviews of Geophysics, 45. doi:10.1029/2005RG000183. 2007.

Frey, H., Machguth, H., Huss, M., Huggel, C., Bajracharya, S., Bolch, T., Kulkarni, A., Linsbauer, A., Salzmann, N. & Stoffel, M. Estimating the volume of glaciers in the Himalayan-Karakoram region using different methods. The Cryosphere, 8, 2313-2333. 2014.

Furbish, D.J. & Andrews, J.T. The use of hypsometry to indicate long term stability and response of valley glaciers to changes in mass transfer. Journal of Glaciology, 30, 105, 199-211.

Gardelle, J., Arnaud, Y. & Berthier, E. Contrasted evolution of glacial lakes along the Hindu Kush Himalaya mountain range between 1990 and 2009. Global and Planetary Change, 75, 47-55. 2011.

Gardelle, J., Berthier, E., Arnaud, Y. & Kääb, A. Region-wide glacier mass balances over the Pamir-Karakoram-Himalaya during 1999-2011. Cryosphere, 7, 1263-1286. 2013.

Hambrey, M. J., Quincey, D. J., Glasser, N. F., Reynolds, J. M., Richardson, S. J. & Clemmens, S. Sedimentological, geomorphological and dynamic context of debris-mantled glaciers, Mount Everest (Sagarmatha) region, Nepal. Quaternary Science Reviews, 27, 2361-2389. 2008.

Huss, M. & Hock, R. A new model for global glacier change and sea-level rise. Frontiers in Earth Science, 3. 2015.

Immerzeel, W. W., Van Beek, L. P. H. & Bierkens, M. F. P. Climate Change Will Affect the Asian Water Towers. Science, 328, 1382-1385. 2010.

Jin, R., Li, X., Che, T., WU, L. & Mool, P. Glacier area changes in the Pumqu river basin, Tibetan Plateau, between the 1970s and 2001. Journal of Glaciology, 51, 607-610. 2005.

Jiskoot, H., Curran, C. J., Tessler, D. L. & Shenton, L. R. Changes in Clemenceau Icefield and Chaba Group glaciers, Canada, related to hypsometry, tributary detachment, length, slope and area & aspect relations. Annals of Glaciology, 50, 133-143. 2009.

Kääb, A. Combination of SRTM3 and repeat ASTER data for deriving alpine glacier flow velocities in the Bhutan Himalaya. Remote Sensing of Environment, 94, 463-474. 2005.

Kääb, A., Berthier, E., Nuth, C., Gardelle, J. & Arnaud, Y. Contrasting patterns of early twenty-first-century glacier mass change in the Himalayas. Nature, 488, 495-498. 2012.

Kapnick, S. B., Delworth, T. L., Ashfaq, M., Malyshev, S. & Milly, P. C. D. Snowfall less sensitive to warming in Karakoram than in Himalayas due to a unique seasonal cycle. Nature Geosci, 7, 834-840. 2014.

Kaspari, S., Hooke, R. LeB., Mayewski, P.A., Kang, S.C., Hou, S.G. & Qin, D.H. Snow accumulation rate on Qomolangma (Mount Everest), Himalaya: synchroneity with sites across the Tibetan Plateau on 50-100 year timescales. Journal of Glaciology, 54, 185, 343-352. Doi: 10.3189/002214308784886126. 2008.

Kattel, D. B., Yao, T., Yang, W., Gao, Y. & Tian, L. Comparison of temperature lapse rates from the northern to the southern slopes of the Himalayas. International Journal of Climatology, 35, 4431-4443. 2015.

Khadka, D., Babel, M. S., Shrestha, S. & Tripathi, N. K. Climate change impact on glacier and snow melt and runoff in Tamakoshi basin in the Hindu Kush Himalayan (HKH) region. Journal of Hydrology, 511, 49-60. 2014.

König, M., Nuth, C., Kohler, J., Moholdt, G. & Pettersen, R. A digital glacier database for svalbard. In: Kargel, S. J., Leonard, J. G., Bishop, P. M., Kääb, A. & Raup, H. B. (eds.) Global Land Ice Measurements from Space. Berlin, Heidelberg: Springer Berlin Heidelberg. 2014.

Larsen, C. F., Motyka, R. J., Arendt, A. A., Echelmeyer, K. A. & Geissler, P. E. Glacier changes in southeast Alaska and northwest British Columbia and contribution to sea level rise. Journal of Geophysical Research: Earth Surface, 112, F01007. 2007.

Liu, Shiyin (submitter); Liu, Shiyin; Guo, Wanqin (analyst(s)). GLIMS Glacier Database. Boulder, CO. National Snow and Ice Data Center. 2014.

Lutz, A. F., Immerzeel, W. W., Gobiet, A., Pellicciotti, F. & Bierkens, M. F. P. Comparison of climate change signals in CMIP3 and CMIP5 multi-model ensembles and implications for Central Asian glaciers. Hydrol. Earth Syst. Sci., 17, 3661-3677. 2013.

Pepin, N., Bradley, R.S., Diaz, H.F., Baraer, M., Caceres, E.B., Forsythe, N., Fowler, G., Greenwood, M.Z., Hashmi, X.D., Liu, J.R., Miller, K., Ning, A., Ohmura, E., Palazzi, I., Rangwala, W., Schöner, I., Seversky, M., Shahgedanova, M., Wang, S.N. Williamson, N. & Yang, D.Q. Elevation-dependent warming in mountain regions of the world. Nature Clim. Change, 5, 424-430. 2015.

Noh, M. J. & Howat, I. M. Automated stereo-photogrammetric DEM generation at high latitudes: Surface Extraction with TIN-based Search-space Minimization (SETSM) validation and demonstration over glaciated regions. GIScience & Remote Sensing, 52, 198-217. 2015.

Nuimura, T., Fujita, K., Yamaguchi, S. & Sharma, R. R. Elevation changes of glaciers revealed by multitemporal digital elevation models calibrated by GPS survey in the Khumbu region, Nepal Himalaya, 1992-2008. Journal of Glaciology, 58, 648-656. 2012.

Nuth, C. & Kääb, A. Co-registration and bias corrections of satellite elevation data sets for quantifying glacier thickness change. Cryosphere, 5, 271-290. 2011.

Nuth, C., Kohler, J., Aas, H. F., Brandt, O. & Hagen, J. O. Glacier geometry and elevation changes on Svalbard (1936-90): a baseline dataset. In: SHARP, M. (ed.) Annals of Glaciology, Vol 46, 2007. Cambridge: Int Glaciological Soc. 2007.

Owen, L.A. Robinson, R., Benn, D.I., Finkel, R.C., Davis, N.K., Yi, C., Putkonen, J., Li, D. & Murray, A.S. Quaternary glaciation of Mount Everest. *Quaternary Science Reviews*, 28(15-16), pp.1412–1433. 2009.

Pellicciotti, F., Stephan, C., Miles, E., Herreid, S., Immerzeel, W. W. & Bolch, T. Mass-balance changes of the debris-covered glaciers in the Langtang Himal, Nepal, from 1974 to 1999. Journal of Glaciology, 61, 373-386. 2015.

Quincey, D. J., Luckman, A. & Benn, D. Quantification of Everest region glacier velocities between 1992 and 2002, using satellite radar interferometry and feature tracking. Journal of Glaciology, 55, 596-606. 2009.

Quincey, D. J., Richardson, S. D., Luckman, A., Lucas, R. M., Reynolds, J. M., Hambrey, M. J. & Glasser, N. F. Early recognition of glacial lake hazards in the Himalaya using remote sensing datasets. Global and Planetary Change, 56, 137-152. 2007.

Racoviteanu, Adina (submitter); Bajracharya, Samjwal (analyst(s)). GLIMS Glacier Database. Boulder, CO. National Snow and Ice Data Center. 2008.

Reynolds, J.M. Glacial hazard assessment at Tsho Rolpa, Rolwaling, Central Nepal. Quaterly Journal of Engineering Geology and Hydrogeology, 32, 209-214. 1999.

Rignot, E., Echelmeyer, K. & Krabill, W. Penetration depth of interferometric synthetic-aperture radar signals in snow and ice. Geophysical Research Letters, 28, 3501-3504. 2001.

Rounce, D. R. & Mckinney, D. C. Debris thickness of glaciers in the Everest area (Nepal Himalaya) derived from satellite imagery using a nonlinear energy balance model. The Cryosphere, 8, 1317-1329. 2014.

Rowan, A. V., Egholm, D. L., Quincey, D. J. & Glasser, N. F. Modelling the feedbacks between mass balance, ice flow and debris transport to predict the response to climate change of debris-covered glaciers in the Himalaya. Earth and Planetary Science Letters, 430, 427-438. 2015.

Rupper, S., Schaefer, J.M., Burgener, L.K., Koenig, L.S., Tsering, K. & Cook, E.R. Sensitivity and response of Bhutanese glaciers to atmospheric warming. *Geophysical Research Letters*, 39(19), p.L19503. 2012.

Sakai, A., Chikita, K. & Yamada, T. Expansion of a moraine-dammed glacial lake, Tsho Rolpa, in Rolwaling Himal, Nepal Himalaya. Limnology and Oceanography, 45, 1401-1408. 2000.

Salerno, F., Guyennon, N., Thakuri, S., Viviano, G., Romano, E., Vuillermoz, E., Cristofanelli, P., Stocchi, P., Agrillo, G., Ma, Y. & Tartari, G. Weak precipitation, warm winters and springs impact glaciers of south slopes of Mt. Everest (central Himalaya) in the last 2 decades (1994–2013). The Cryosphere, 9, 1229-1247. 2015.

Shrestha, A. B., Wake, C. P., Mayewski, P. A. & Dibb, J. E. Maximum temperature trends in the Himalaya and its vicinity: An analysis based on temperature records from Nepal for the period 1971-94. Journal of Climate, 12, 2775-2786. 1999.

Somos-Valenzuela, M. A., Mckinney, D. C., Rounce, D. R. & Byers, A. C. Changes in Imja Tsho in the Mount Everest region of Nepal. Cryosphere, 8, 1661-1671. 2014.

Thakuri, S., Salerno, F., Smiraglia, C., Bolch, T., D'Agata, C., Viviano, G. & Tartari, G. Tracing glacier changes since the 1960s on the south slope of Mt. Everest (central Southern Himalaya) using optical satellite imagery. Cryosphere, 8, 1297-1315. 2014.

USGS. 2016. *Shuttle Radar Topography Mission (SRTM) 1 Arc-Second Global*. [ONLINE] Available at: https://lta.cr.usgs.gov/SRTM1Arc. [Accessed 08 March 2016]

Vuichard, D. & Zimmerman, M. The 1985 Catastrophic Drainage of a Moraine-Dammed Lake, Khumbu Himal, Nepal: Cause and Consequences. Mountain Research and Development, 7, 91-110. 1987.

Watson, C.S. Quincey, D.J, Carrivick, J.L. and Smith, M.W. The dynamics of supraglacial ponds in the Everest region, central Himalaya. Global and Planetary Change, 142, 14-27. 2016.

Yang, X., Zhang, T., Qin, D., Kang, S. & Qin, X. Characteristics and Changes in Air Temperature and Glacier's Response on the North Slope of Mt. Qomolangma (Mt. Everest). Arctic, Antarctic, and Alpine Research, 43, 147-160. 2011.

Ye, Q., Bolch, T., Naruse, R., Wang, Y., Zong, J., Wang, Z., Zhao, R., Yang, D. & Kang, S. Glacier mass changes in Rongbuk catchment on Mt. Qomolangma from 1974 to 2006 based on topographic maps and ALOS PRISM data. Journal of Hydrology, 530, 273-280. 2015.

The Cryosphere Discuss., doi:10.5194/tc-2016-99, 2016
Manuscript under review for journal The Cryosphere
Published: 23 May 2016

Table 1. Scenes used in glacier outline delineation, ASTER DEM generation and by the Polar Geospatial Centre in the generation of SETSM DEMs.

Sensor	Scene ID	Date of acquisition	Purpose
Landsat OLI	LC81400412014334LGN00	30/11/2014	Glacier outlines
Landsat ETM+	LE71390412000302SGS00	29/10/2000	Glacier outlines
ASTER	L1A.003:2014050545	29/11/2014	ASTER DEM
ASTER	L1A.003:2014045939	12/04/2014	ASTER DEM
Worldview 3	WV03_20150121_10400100076C0700	21/01/2015	SETSM DEM
Worldview 1	WV01_20150504_102001003C5FB900	04/05/2015	SETSM DEM
Worldview 1	WV01_20140115_102001002A289F00	15/01/2014	SETSM DEM
Worldview 2	WV02_20140311_103001002E546F00	11/03/2014	SETSM DEM
Worldview 1	WV01_20140324_102001002D263400	24/03/2014	SETSM DEM
Worldview 1	WV01_20150204_102001003A5B7900	04/02/2015	SETSM DEM
Worldview 2	WV02_20150202_103001003D4C7900	02/02/2015	SETSM DEM
Worldview 1	WV01_20140218_102001002C5FA100	18/02/2014	SETSM DEM
Worldview 1	WV01_20141022_102001003525D400	22/10/2014	SETSM DEM
Worldview 1	WV01_20150131_1020010038618500	31/01/2015	SETSM DEM
Worldview 2	WV02_20141226_103001001D66C000	26/12/2014	SETSM DEM
Worldview 2	WV02_20141110_1030010039013C00	10/11/2014	SETSM DEM
Worldview 1	WV01_20141129_102001002776B500	29/11/2014	SETSM DEM
Worldview 1	WV01_20140514_102001003001E400	14/05/2014	SETSM DEM

The Cryosphere Discuss., doi:10.5194/tc-2016-99, 2016
Manuscript under review for journal The Cryosphere
Published: 23 May 2016

Table 2. Glaciers highlighted in the study. Data on glacier area and altitudinal range are taken from the GLIMS database. Glacier length is measured along centrelines from the bergschrund. Catchment notation: TK- Tama Koshi; DK- Dudh Koshi; TP- Tibetan Plateau; TP clean (surface debris-free) glaciers on the Tibetan Plateau.

				Altitude (m)				
GLIMS ID	Name	Length (km)	Area (km^2)	Min	Max	Range	Lake status	Catchment
G086218E28282N	Bamolelingja	7.4	15.4	5013	6745	1732	No lake	TK
G086280E28276N	G1	12.3	42.7	4778	7045	2467	No lake	TK
G086550E28133N	Yanong	3.4	4.4	4984	6377	1393	Proglacial lake	TK
G086548E28174N	Yanong North	3.2	4.1	5025	6524	1499	Proglacial lake	TK
G086384E28259N	Erbu	10.9	25.8	5020	7130	2310	No lake	TK
G086471E27959N	Drogpa Nagtsang	8.2	25.3	5018	7031	2013	Supraglacial lake	TK
G086537E27874N	Trakarding	17.7	35.4	4561	6659	2098	Proglacial lake	TK
G086519E27919N	Ripimo Shar	10.3	19.7	4600	6683	2083	No lake	TK
G086533E28088N	Shalong	7.9	18.4	5301	6835	1534	No lake	TK
G086771E28015N	Ngozumpa	22.2	80.7	4686	8176	3490	Supraglacial lake	DK
G086949E27913N	Imja	6.5	15.3	5021	7998	2977	Supraglacial lake	DK
G086820E27978N	Khumbu	15.7	39.5	4915	8062	3147	Coalescing ponds	DK
G086625E28029N	Lumbsamba	9.1	12.5	4936	7258	2322	No lake	DK
G086917E27925N	Lhotse	7.1	6.9	4821	6082	1261	No lake	DK
G086541E27988N	Melung	6.5	7.6	5271	6028	757	No lake	DK
G086587E28039N	Bhote Kosi	14.4	28.4	4793	6679	1886	No lake	DK
G086900E27843N	Hungu	4.7	13.9	5207	6942	1735	Proglacial lake	DK
G086900E27843N	Marala	2.9	13.9	5366	5920	554	Proglacial lake	DK
G086798E28111N	Jiuda	10.1	15.9	5405	7801	2396	No lake	TP
G086719E28132N	Gyachung	13.6	47.1	5309	7853	2544	No lake	TP
G086939E28060N	Rongbuk East	10.9	26.7	5640	8361	2721	No lake	TP
G086866E28050N	Rongbuk	19.5	73.2	5153	8758	3605	Supraglacial lake	TP
G086466E28321N	Ayi	8.6	7.27	5313	6863	1550	Coalescing ponds	TP
G086456E28291N	Tibet 1	12.9	26.8	5138	7085	1947	Coalescing ponds	TP
G086633E28122N	Gyabrag	11.5	33.2	5095	8182	3087	No lake	TP
G086235E28330N	Longmojian	4.5	9.3	5348	6788	1440	Proglacial lake	TP
G086382E28331N	Duiya	9.3	22.5	5480	7201	1721	Proglacial lake	TP
G086395E28347N	Duosangpuxi	5.5	7.7	5561	6992	1431	No lake	TP clean
G086657E28179N	Siguang	5.2	5.8	5652	6866	1214	No lake	TP clean
G086423E28367N	Duosangudong	6.3	8.8	5502	6925	1423	No lake	TP clean
G086709E28242N	G08	3.8	6.4	5726	6475	749	No lake	TP clean
G086275E28322N	G06	6.0	6.0	5545	6926	1381	No lake	TP clean

The Cryosphere Discuss., doi:10.5194/tc-2016-99, 2016
Manuscript under review for journal The Cryosphere
Published: 23 May 2016

Table 3. Mean differences and the standard deviation associated with off-glacier elevation difference data between ASTER, SETSM and SRTM DEMs before and after the DEM correction process. The standard error of elevation differences is also listed.

Sensor	ASTER scene ID	Pre correction mean & StDev stable ground differences Vs SRTM (m)	Post correction mean & StDev stable ground differences Vs SRTM (m)	St. error (m a^{-1})
ASTER	L1A.003:2014050545	–64.12, 25.99	0.43, 17.40	0.44
ASTER	L1A.003:2014045939	–22.83, 34.72	–0.27, 23.18	0.32
	SETSM tile			
Worldview 3	WV03_20150121_10400100076C0700	–37.37, 11.44	0.53, 8.44	0.56
Worldview 1	WV01_20150504_102001003C5FB900	–40.77, 14.11	–0.43, 5.53	0.44
Worldview 1	WV01_20140115_102001002A289F00	–32.76, 7.41	0.50, 6.60	0.50
Worldview 2	WV02_20140311_103001002E546F00	–44.13, 15.57	–0.13, 9.13	0.21
Worldview 1	WV01_20140324_102001002D263400	–30.84, 8.56	0.07, 6.85	0.08
Worldview 1	WV01_20150204_102001003A5B7900	–54.28, 18.09	–0.36, 8.30	0.38
Worldview 2	WV02_20150202_103001003D4C7900	–34.00, 12.81	–0.03, 7.45	0.06
Worldview 1	WV01_20140218_102001002C5FA100	–32.16, 9.78	–0.23, 6.85	0.23
Worldview 1	WV01_20141022_102001003525D400	–40.88, 14.81	0.36, 8.64	0.41
Worldview 1	WV01_20150131_1020010038618500	–38.99, 22.37	–0.83, 8.43	0.83
Worldview 2	WV02_20141110_1030010039013C00	–26.61, 7.70	0.07, 6.85	0.08
Worldview 1	WV01_20141129_102001002776B500	–34.06, 6.05	0.16, 4.99	0.16
Worldview 1	WV01_20140514_102001003001E400	–32.33, 9.17	–0.26, 6.54	0.26

The Cryosphere Discuss., doi:10.5194/tc-2016-99, 2016
Manuscript under review for journal The Cryosphere
Published: 23 May 2016

Table 4. Mean and maximum (across one, 100 m altitudinal band) surface lowering rates and estimates of mass loss from below ELAs of glaciers included in the study. Bold text indicates lacustrine-terminating glaciers; means are italicised.

Glacier	Mean SL rate (m a^{-1})	Maximum SL rate (m a^{-1})	Mean mass loss m w.e. a^{-1}	Catchment
Bamolelingja	–0.58 ± 0.33	–1.50 ± 0.33	–0.55 ± 0.35	TK
G1	–0.47 ± 0.18	–1.25 ± 0.18	–0.40 ± 0.18	TK
Yanong	**–1.55 ± 0.26**	**–3.78 ± 0.26**	**–1.48 ± 0.35**	**TK**
Yanong North	**–1.13 ± 0.26**	**–3.06 ± 0.26**	**–1.00 ± 0.33**	**TK**
Erbu	–0.50 ± 0.18	–0.73 ± 0.18	–0.52 ± 0.20	TK
Drogpa Nagtsang	**–0.78 ± 0.66**	**–1.91 ± 0.66**	**–0.70 ± 0.67**	**TK**
Trakarding	**–0.94 ± 0.54**	**–2.19 ± 0.54**	**–0.84 ± 0.56**	**TK**
Ripimo Shar	–0.72 ± 0.54	–0.97 ± 0.54	–0.66 ± 0.56	TK
Shalong	–0.52 ± 0.26	–0.96 ± 0.26	–0.47 ± 0.27	TK
Mean	*–0.80 ± 0.36*	*–1.81 ± 0.36*	*–0.73 ± 0.39*	
Ngozumpa	–0.64 ± 0.48	–1.17 ± 0.48	–0.62 ± 0.49	DK
Imja	**–0.84 ± 0.51**	**–1.62 ± 0.51**	**–0.80 ± 0.31**	**DK**
Khumbu	–0.84 ± 0.16	–1.34 ± 0.16	–0.81 ± 0.17	DK
Lumbsamba	–0.31 ± 0.26	–0.89 ± 0.26	–0.29 ± 0.26	DK
Lhotse	–0.66 ± 0.51	–0.99 ± 0.51	–0.68 ± 0.30	DK
Melung	–0.40 ± 0.42	–1.12 ± 0.42	–0.40 ± 0.28	DK
Bhote Kosi	–0.72 ± 0.42	–1.33 ± 0.42	–0.67 ± 0.29	DK
Hungu	**–0.54 ± 0.31**	**–1.10 ± 0.31**	**–0.50 ± 0.29**	**DK**
Marala	**–0.61 ± 0.31**	**–2.24 ± 0.31**	**–0.56 ± 0.29**	**DK**
Mean	*–0.62 ± 0.27*	*–0.95 ± 0.27*	*–0.57 ± 0.33*	
Jiuda	–0.64 ± 0.16	–1.33 ± 0.16	–0.62 ± 0.18	TP
Gyachung	–0.66 ± 0.54	–1.07 ± 0.54	–0.61 ± 0.56	TP
Rongbuk East	–1.04 ± 0.26	–2.45 ± 0.26	–0.98 ± 0.32	TP
Rongbuk	–1.31 ± 0.18	–2.02 ± 0.18	–1.30 ± 0.24	TP
Ayi	–0.68 ± 0.66	–1.45 ± 0.66	–0.53 ± 0.59	TP
Tibet 1	–1.17 ± 0.18	–2.14 ± 0.18	–1.36 ± 0.30	TP
Gyabrag	–1.22 ± 0.26	–3.40 ± 0.26	–1.21 ± 0.32	TP
Longmojian	**–1.12 ± 0.33**	**–2.53 ± 0.33**	**–0.99 ± 0.39**	**TP**
Duiya	**–0.65 ± 0.18**	**–1.45 ± 0.18**	**–0.66 ± 0.22**	**TP**
Mean	*–0.95 ± 0.30*	*–1.98 ± 0.30*	*–0.92 ± 0.36*	
Duosangpuxi	–0.53 ± 0.18	–1.30 ± 0.18	–0.52 ± 0.21	TP-clean
Siguang	–0.61 ± 0.54	–1.06 ± 0.54	–0.59 ± 0.57	TP-clean
Duosangudong	–0.31 ± 0.66	–0.91 ± 0.66	–0.32 ± 0.67	TP-clean
G08	–0.49 ± 0.54	–0.96 ± 0.54	–0.47 ± 0.56	TP-clean
G06	–0.51 ± 0.18	–0.98 ± 0.18	–0.49 ± 0.19	TP-clean
Mean	*–0.49 ± 0.42*	*–1.04 ± 0.52*	*–0.47 ± 0.44*	

5

The Cryosphere Discuss., doi:10.5194/tc-2016-99, 2016
Manuscript under review for journal The Cryosphere
Published: 23 May 2016

Table 5. Hypsometric Index (HI) scores and classification, accumulation area ratio (AAR) and total area loss for each glacier included in the study. The ELA of the Lhotse and Melung glaciers are now above their altitudinal ranges, thus AARs cannot be calculated. Catchments: TK- Tama Koshi; DK- Dudh Koshi; TP- Tibetan Plateau. Lacustrine terminating glaciers are in bold; mean values are italicised.

Glacier	HI score	HI classification	AAR	Area change (km^2 (% of total))	Approximate ELA (m)	Catchment
Bamolelingja	0.91	Equidimensional	0.23	0.07 (0.44%)	5800	TK
G1	1.45	Bottom heavy	0.35	0.49 (1.15%)	5900	TK
Yanong	**0.94**	**Equidimensional**	**0.54**	**0.31 (6.33%)**	**5500**	TK
Yanong North	**1.22**	**Equidimensional**	**0.54**	**0.16 (4.07%)**	**5500**	TK
Erbu	1.15	Equidimensional	0.39	0.05 (0.24%)	5700	TK
Drogpa Nagtsang	**1.18**	**Equidimensional**	**0.22**	**2.37 (9.12%)**	**5800**	TK
Trakarding	**0.69**	**Equidimensional**	**0.39**	**0.35 (0.98%)**	**5800**	TK
Ripimo Shar	0.98	Equidimensional	0.40	0.04 (0.20%)	5600	TK
Shalong	1.21	Bottom heavy	0.25	0.09 (0.45%)	5500	TK
Mean	*1.14*	*Equidimensional*	*0.36*	*0.43 (2.55%)*	*5677*	
Ngozumpa	2.62	Very bottom heavy	0.61	0.13 (0.16%)	5700	DK
Imja	**5.93**	**Very bottom heavy**	**0.34**	**0.5 (3.21%)**	**5600**	DK
Khumbu	3.95	Very bottom heavy	0.59	0.06 (0.22%)	5800	DK
Lumbsamba	3.11	Very bottom heavy	0.32	0.02 (0.15%)	5800	DK
Lhotse	1.93	Very bottom heavy	-	0 (0%)	-	DK
Melung	1.52	Very bottom heavy	-	0.2 (2.55%)	-	DK
Bhote Kosi	2.36	Very bottom heavy	0.15	0.13 (0.51%)	5700	DK
Hungu	**1.69**	**Very bottom heavy**	**0.41**	**0.13 (1.53%)**	**5900**	DK
Marala	**0.56**	**Equidimensional**	**0.21**	**0.11 (2.2%)**	**5800**	DK
Mean	*2.63*	*Very bottom heavy*	*0.37*	*0.14 (1.17%)*	*5757*	
Jiuda	1.45	Bottom heavy	0.51	0.1 (0.62%)	6300	TP
Gyachung	1.85	Very bottom heavy	0.34	0.06 (0.21%)	6300	TP
Rongbuk East	2.58	Very bottom heavy	0.61	0.8 (2.85%)	6400	TP
Rongbuk	3.25	Very bottom heavy	0.25	0.14 (0.16%)	5900	TP
Ayi	3.00	Very bottom heavy	0.14	0.31 (3.90%)	5900	TP
Tibet 1	2.80	Very bottom heavy	0.27	0.35 (1.38%)	5800	TP
Gyabrag	2.83	Very bottom heavy	0.53	1.17 (3.32%)	5800	TP
Longmojian	**3.09**	**Very bottom heavy**	**0.16**	**0.44 (4.28%)**	**5800**	TP
Duiya	**1.39**	**Bottom heavy**	**0.70**	**0.50 (2.07%)**	**6100**	TP
Mean	*2.47*	*Very bottom heavy*	*0.40*	*0.39 (1.91%)*	*6033*	
Duosangpuxi	1.23	Bottom heavy	0.29	0.16 (2.07%)	6100	TP clean
Siguang	1.03	Equidimensional	0.19	0.06 (1.03%)	6000	TP clean
Duosangpudong	1.19	Equidimensional	0.26	0.10 (1.13%)	6000	TP clean
G08	0.76	Top heavy	0.39	0.07 (1.09%)	6100	TP clean
G06	1.73	Very bottom heavy	0.31	0.08 (1.25%)	5900	TP clean
Mean	*1.18*	*Equidimensional*	*0.29*	*0.09 (1.31%)*	*6020*	

The Cryosphere Discuss., doi:10.5194/tc-2016-99, 2016
Manuscript under review for journal The Cryosphere
Published: 23 May 2016

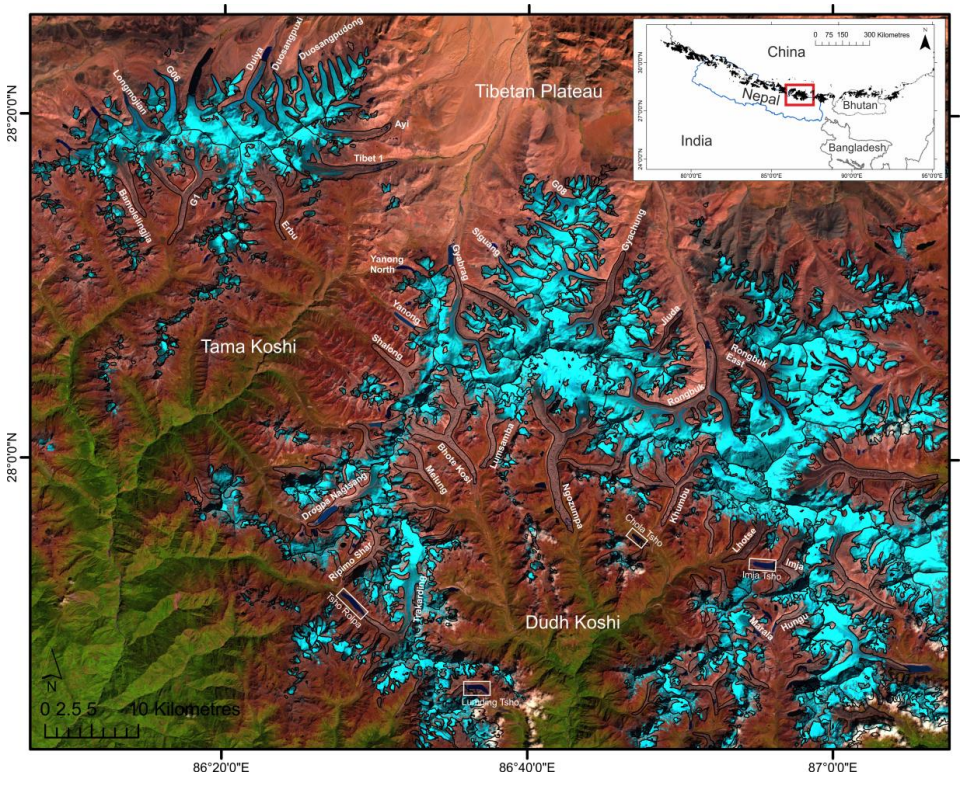

Figure 1. The glaciers of the Everest region. Named glaciers are the glaciers we highlight in this study. Major catchments include the Tama Koshi and Dudh Koshi on the southern flank of the Himalaya and the Pumqu river catchment on the northern side of the divide, with glaciers flowing onto the Tibetan Plateau (China). Named glacial lakes are highlighted, although many remain unnamed.

The Cryosphere Discuss., doi:10.5194/tc-2016-99, 2016
Manuscript under review for journal The Cryosphere
Published: 23 May 2016

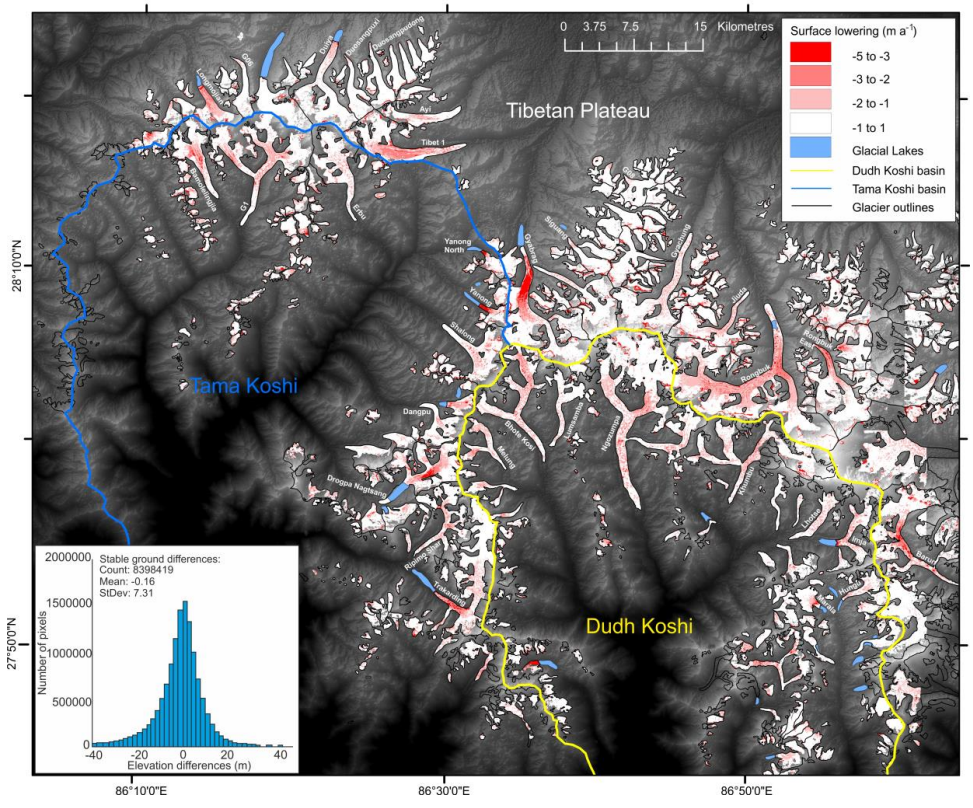

Figure 2. Glacier surface lowering over the study area between 2000 and 2014/15. Also shown is a summary of off-glacier terrain differences.

The Cryosphere Discuss., doi:10.5194/tc-2016-99, 2016
Manuscript under review for journal The Cryosphere
Published: 23 May 2016

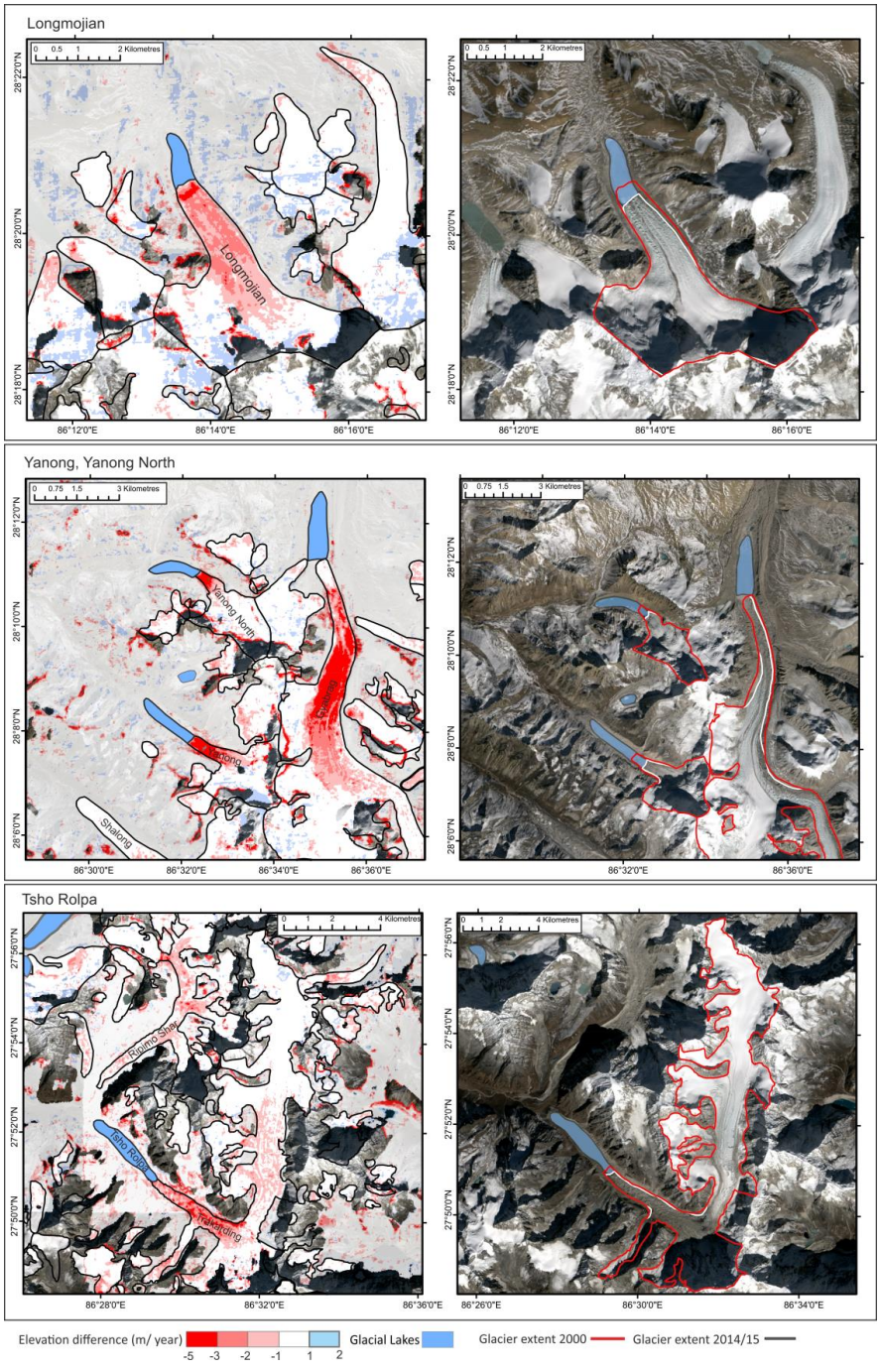

Figure 3. Examples of surface lowering and total area change over the study period on lacustrine terminating glaciers. Semi-transparent, off-glacier differences are also shown.

The Cryosphere Discuss., doi:10.5194/tc-2016-99, 2016
Manuscript under review for journal The Cryosphere
Published: 23 May 2016

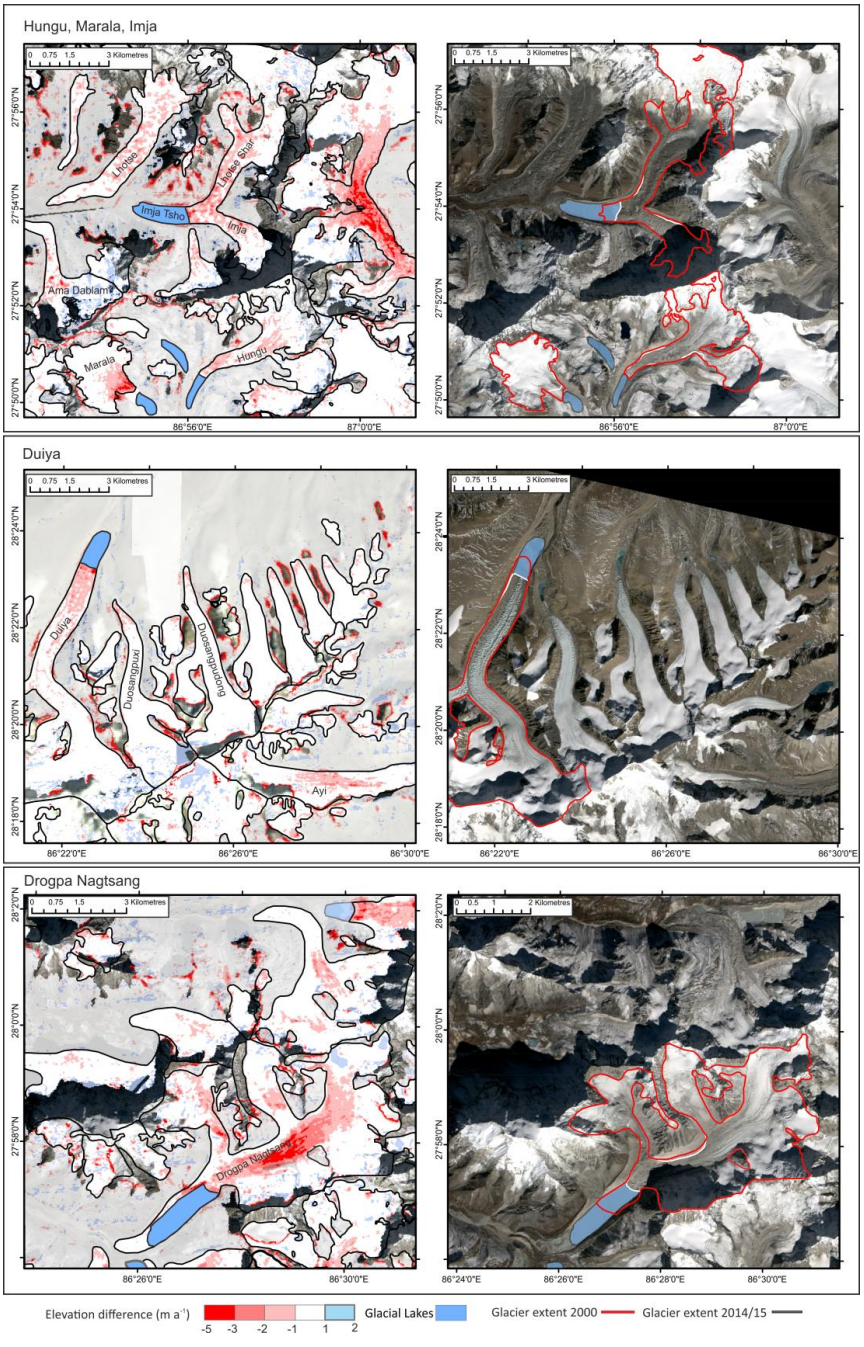

Figure 4. Further examples of surface lowering and total area change over the study period on lacustrine terminating glaciers. Semi-transparent, off-glacier differences are also shown.

The Cryosphere Discuss., doi:10.5194/tc-2016-99, 2016
Manuscript under review for journal The Cryosphere
Published: 23 May 2016

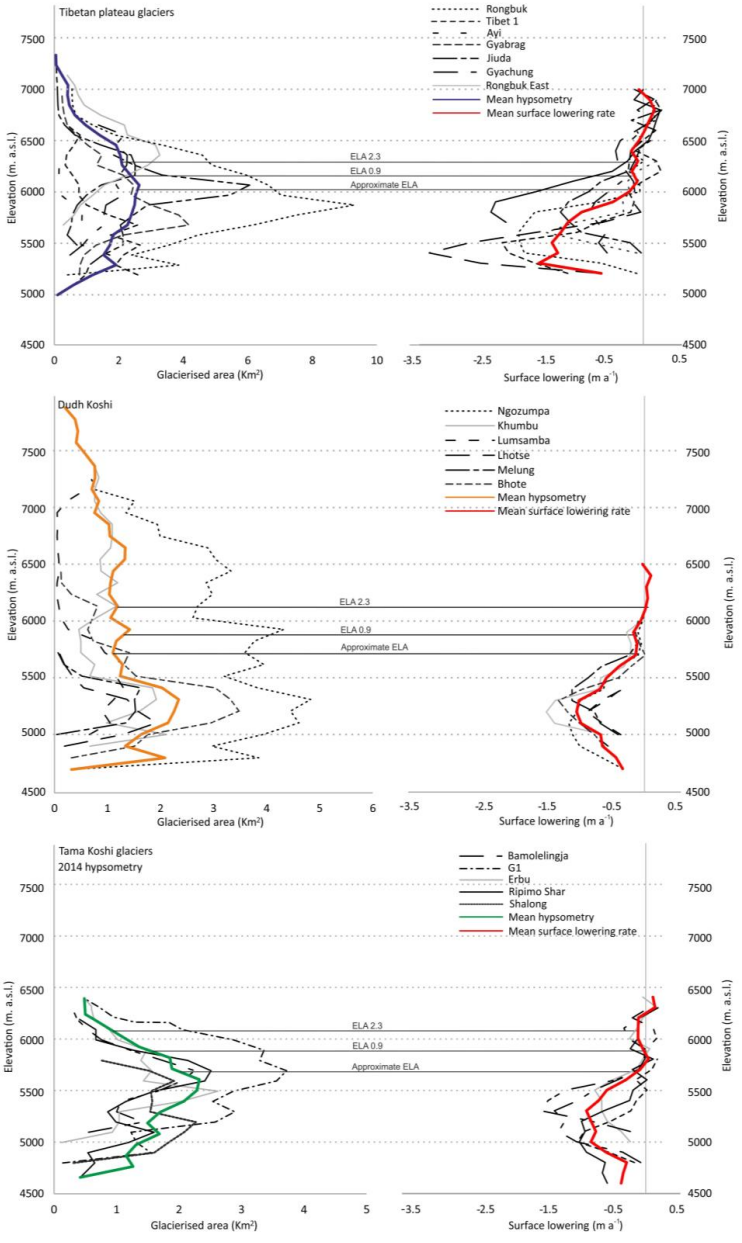

Figure 5. Surface lowering and glacier hypsometry curves for all land terminating glaciers in the three different catchments of the study area. Approximate equilibrium line altitudes (ELA) for the study period and for different scenarios of warming (0.9 and 2.3 ºC) are also shown.

The Cryosphere Discuss., doi:10.5194/tc-2016-99, 2016
Manuscript under review for journal The Cryosphere
Published: 23 May 2016

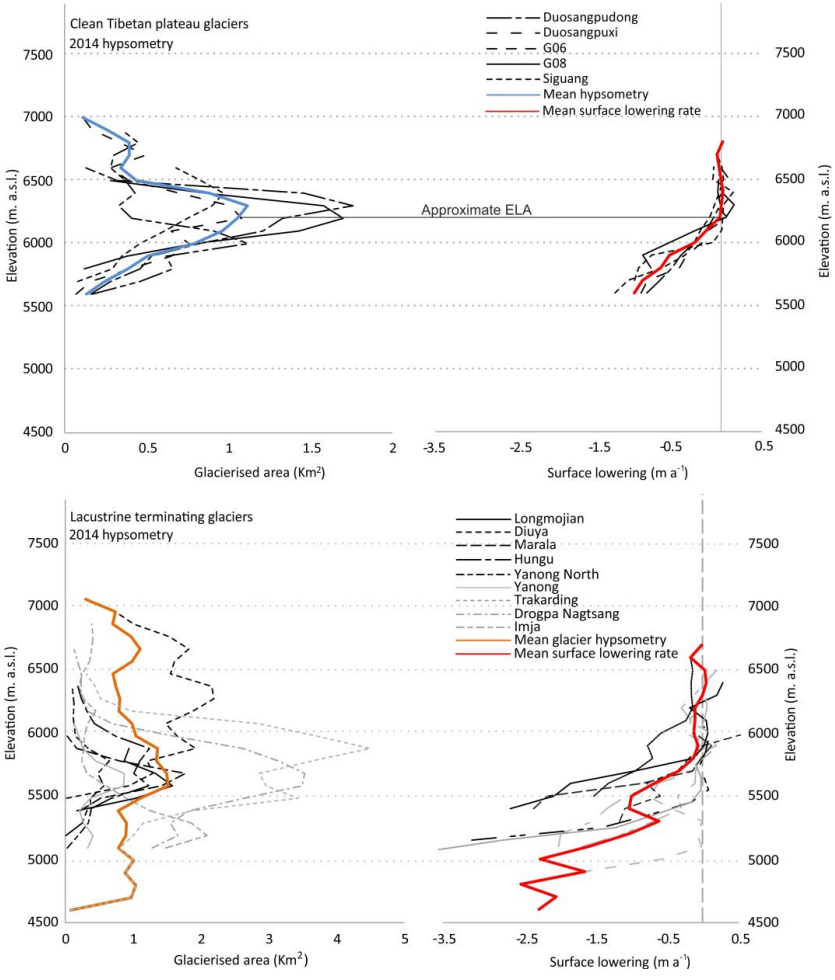

Figure 6. Surface lowering and glacier hypsometry curves for clean ice and lacustrine terminating glaciers in the study area.

The Cryosphere Discuss., doi:10.5194/tc-2016-99, 2016
Manuscript under review for journal The Cryosphere
Published: 23 May 2016

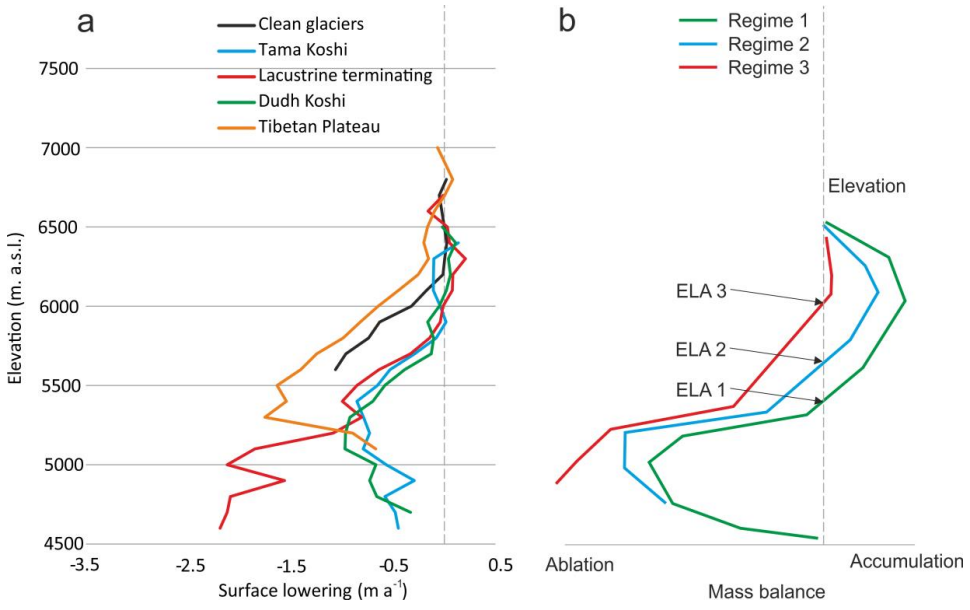

Figure 7. A- Surface lowering curves for land terminating glaciers averaged across each catchment and for the populations of clean ice and lacustrine terminating glaciers we highlight. B- Mass balance curves proposed by Benn et al. (2012) to represent three distinct regimes of ice melt on debris-covered glaciers.

5